RSC Advances

PAPER

View Article Online
View Journal | View Issue

Cite this: *RSC Adv.*, 2017, **7**, 14314

Solvent free mechanochemical synthesis of Eu^{3+} complex and its luminescent sensing of trace water and temperature†

Daqing Yang, Zhiqiang Li, Liang He, Yucheng Deng and Yige Wang*

Mechanochemical transduction processes which translate macroscopic forces into chemical reactions are a design method to synthesize new advanced functional materials. Herein we present a simple, facile and solventless method for the formation of a Eu^{3+} coordination complex by simply grinding 4′,4‴′-(1,4-phenylene)bis(2,2′:6′,2″-terpyridine) and $EuCl_3 \cdot 6H_2O$ in a mortar for a short time. The resulting complex exhibits outstanding stimuli-responsive emissions for temperature and trace water in organic solvents. The ratiometric luminescence determination method based on the emission intensity ratio of two independent transitions of Eu^{3+} provides a way to rapidly detect traces of water (0.1–5% v/v) in various organic solvents through the luminescence quenching mechanism. Furthermore, by virtue of the temperature-dependent luminescent behavior, the complex allows for the design of a thermometer with an excellent linear response to temperature over a wide range, from 80 to 420 K with a high relative sensitivity of 0.52% per K at 300 K and an unprecedented high sensitivity of 10.26% per K at 420 K. The dynamically reversible complexation between Eu^{3+} and the ligand facilitates its application as a smart material.

Received 12th December 2016
Accepted 24th February 2017

DOI: 10.1039/c6ra28099d

rsc.li/rsc-advances

1. Introduction

The luminescence of trivalent lanthanide ions (Ln^{3+}) is especially interesting as they typically show highly desirable physical properties such as sharp emission lines, long lifetimes, high quantum yields and large Stocks shifts, making them suitable for a variety of advanced photonic applications.[1–4] However, the emission intensities of bare lanthanide ions are weak because of the forbidden nature of the f–f transitions. This problem can be addressed by coordinating Ln^{3+} to organic ligands bearing the suitable light-absorbing chromophores *via* the so-called antenna effect.[5,6] Ln^{3+} complexes are normally obtained by the coordinative interactions between metal ions and organic ligands. They have attracted the attention of researchers across various fields due to their versatile structure, morphology and physical properties as well as their unique redox, optical, electronic, catalytic and magnetic properties induced by the incorporated metal ions.[7–14] Tridentate terpyridine ligands can act as efficient Ln^{3+} emission sensitizers and as organic linkers suitable for constructing the Ln^{3+} complexes.[15–18] Various luminescence materials were prepared by a self-assembly process between Ln^{3+} and tridentate terpyridine ligands. In addition to interesting luminescent features such as tunable emission color and white-light emission, these materials are endowed with stimuli-responsive ability and/or self-healability.[13,19–24] Furthermore, the morphology of the Ln^{3+} complexes is highly dependent on the concentration, ligand to metal ratio and the ligand flexibility.[25–27] Their preparation usually needs the use of environmentally hazardous solvents. Mechanochemical synthesis provides alternatives to the conventional solvent-based strategy since they can offer obvious advantages such as the reduction or elimination of solvent use, access to new materials or alternative solid forms, convenience, and shorter reaction times.[28–32] Up to now, a variety of compounds such as metal complexes and metal–organic frameworks (MOFs) have been successfully prepared by solvent-free (or minimal amount of solvent assisted) mechanochemical method.[33–39] However, no reports on the Ln^{3+} complexes induced by complexation of Eu^{3+} with organic linker consisting of terpyridine moieties prepared by mechanochemical method appear in the literature yet, to the best of our knowledge.

Herein we report a rapid, solvent-free, room temperature mechanochemical synthesis of an Eu^{3+} complex by simply grinding 4′,4‴′-(1,4-phenylene)bis(2,2′:6′,2″-terpyridine) (**L**) and $EuCl_3 \cdot 6H_2O$ in a mortar for a fixed time. The complex shows bright red luminescence that is highly sensitive to even low level water in organic solvents and to temperature variation in a wide range from 80 to 470 K. The detection of traces of water (0.1–5% v/v) contained in organic solvents such as ether and THF can be easily achieved through an effective luminescence quenching mechanism due to the replacement of **L** with water molecules

School of Chemical Engineering and Technology, Hebei University of Technology, Tianjin, 300130, China. E-mail: wangyige@hebut.edu.cn

† Electronic supplementary information (ESI) available. See DOI: 10.1039/c6ra28099d

which strongly quench the radiative emission. The temperature dependent luminescent properties allow for the design of a thermometer with an excellent linear response to temperature over a wide range from 80–300 K and 300–420 K with a high relative sensitivity of 0.52% per K at 300 K and an unprecedented high sensitivity of 10.26% per K at 420 K.

2. Results and discussion

2.1 Preparation and characterization

L belongs to the three tridentate ligands family. Its chemical structure and emission spectrum are shown in Fig. 1. Compared with single terpyridine compound, bis-terpyridine can be used to build supramolecular compound flexibly.[40] We successfully prepared the Eu^{3+} complex (denoted as $Eu(\mathbf{L})_n$, n= the molar ratio of Eu^{3+}/**L**) with **L** and $EuCl_3 \cdot 6H_2O$ by the mechanochemical technique within a short time. Upon manual grinding for 10 min, the emission colors of the complex showed obvious change from yellow (Fig. 2b) to bright red (Fig. 2f). The obtained complex shows good solubility in MeOH solution and the bright emission implies the coordination of nitrogen atoms from **L** with Eu^{3+} ions and the sensitization of **L** to the metal ions, which is further confirmed by FT-IR spectra and luminescent data. The bands at 1601 to 1544 cm^{-1} in the FT-IR spectrum of the **L** shown in Fig. 3a are assigned to the pyridine ring of **L**, the strong band at 790 cm^{-1} can be ascribed to the C–C bond between the pyridine rings.[41–43] Upon manual grinding with $EuCl_3 \cdot 6H_2O$ for several minutes, the absorption bands corresponding to the terpyridine moieties of **L** shift to 1605 to 1549 cm^{-1} (Fig. 3b), indicative of the coordination of nitrogen atoms of **L** to Eu^{3+} ions.

The morphology was investigated by scanning electron microscopy (SEM) and the data are shown in Fig. 4. The SEM images reveal that the samples with **L** to Eu^{3+} molar ratio below 3 are mainly consist of micro sized bars (0.2–0.5 μm), which are smaller in size compared with the samples prepared by the conventional solution method. A closer look at the images demonstrates that the bars actually are formed by the aggregation of much smaller nanoparticles. Further increase the molar ratio of **L** to Eu^{3+} to 3 : 1 leads to the formation of sample with totally different morphology (Fig. 4e). The fibrous nature of the Eu^{3+} complexes consisting of long intertwining bundles of strings (0.6–0.8 μm) is evidenced from the typical SEM image. Furthermore, spherical nanoparticles with average size of less than 100 nm are also observed.

The composition and the thermal-stability of the Eu^{3+} complex can be roughly estimated by thermogravimetric (TG) analysis. We take the sample $Eu(\mathbf{L})_1$ as an example. The TG curve (Fig. S1, ESI†) shows 16.6% weight loss up to 480 °C is attributed to the desorption of physically adsorbed water and residual solvents. This indicates the as-synthesized sample has

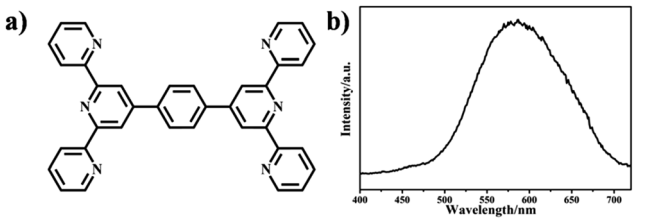

Fig. 1 (a) Chemical structure; (b) emission spectrum excited at 360 nm of L.

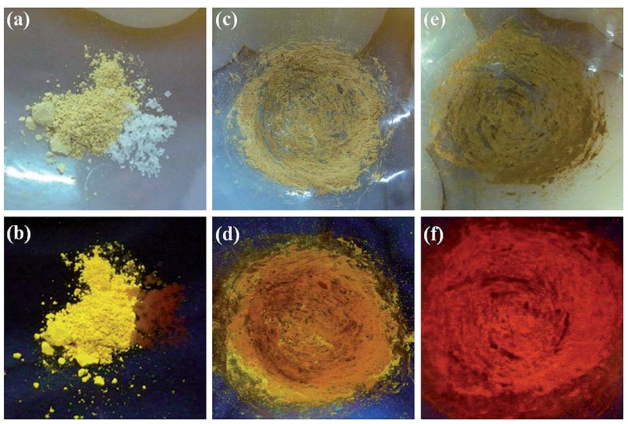

Fig. 2 Bright field and luminescence images under daylight and UV-light showing the process of $Eu(\mathbf{L})_n$ synthesis by the grinding method: (a and b) mixture of L and $EuCl_3 \cdot 6H_2O$, (c and d) the ground mixture after 2 min, and (e and f) the ground mixture after 10 min.

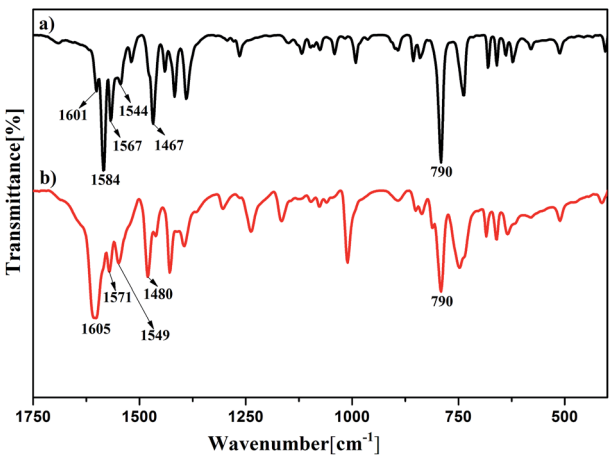

Fig. 3 FT-IR spectra of L (a) and $Eu(L)_1$ (b).

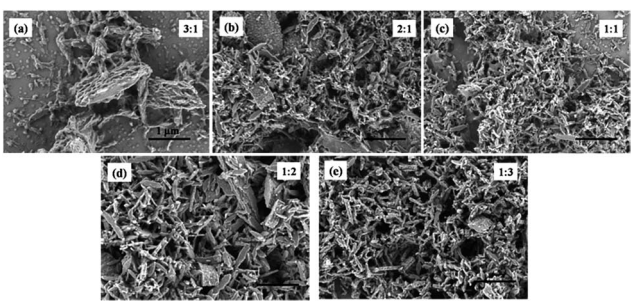

Fig. 4 SEM images of $Eu(\mathbf{L})_n$ in the solid state: (a–e) Eu^{3+} to L ratio from 3 : 1 to 1 : 3.

a high thermal-stability. The second weight loss (*ca.* 47.75%) in the range of 480–720 °C can be ascribed to the decomposition of coordinated ligand.[44] A horizontal thermal curve was observed above 1100 °C, which is due to the formation of the thermally stable product Eu_2O_3 (30.38%). The amount of the chelated europium(III) ions was determined to be 26.24%, and this value roughly corresponds to a molar ratio of 1 : 1 between **L** and Eu^{3+}. To further confirm that the elemental composition of complex, elemental analysis was carried out. Elemental analysis for Eu(**L**)$_1$, found (calcd): C 54.42 (54.1), H 3.13 (3.0), N 10.57 (10.52).

2.2 Optical properties

As shown in Fig. 2f, the final materials prepared by solvent-free mechanochemical synthesis method show bright red-emission when illuminated with a 365 nm UV lamp, indicating the formation of Eu–**L** coordination bonds. We therefore investigate the luminescence properties of the as-synthesized samples, Eu(**L**)$_n$, by steady state and time-resolved emission measurements. Fig. 5 shows the excitation and emission spectra. The broad bands ranging from 250 to 410 nm in all the excitation spectra shown in Fig. 5a are attributed to the absorption of **L**. The emission spectra (Fig. 5b) are formed by a series of line-like bands ascribed to the $^5D_0 \rightarrow {}^7F_J$ ($J = 0, 1, 2, 3$ and 4) transitions of Eu^{3+} with the $^5D_0 \rightarrow {}^7F_2$ transition at 613 nm as the most prominent one, which is responsible for the bright red emission color shown in Fig. 2f. The emission intensity is highly dependent on the molar ratio of **L** to Eu^{3+} ratio. It increases gradually with the molar ratio increasing and reaches the maximum when the molar ratio is 1 : 1, further increasing the molar ratio leads to the gradual decrease of the emission intensity. The luminescence decay curves were measured under excitation at 360 nm and can be well fitted by mono-exponential functions (Fig. S2, ESI†), indicating that only one major emitting species is available in the samples,[45,46] from which the decay time was determined and the data are shown in Table 1. The decay time increases slightly from 0.24 ms to 0.36 ms when the **L** to Eu^{3+} molar ratio increases from 1 : 3 to 1 : 1, further increasing the molar ratio leads to the slight decrease of the decay time, which could be explained by a ligand quenching pathway caused the C–H vibrations of some ligands.[47–49] Furthermore, we also investigated the behavior of the emission intensity ratio $I(^5D_0 \rightarrow {}^7F_2)/I(^5D_0 \rightarrow {}^7F_1)$ (R) of materials. R is typically used to measure the degree of Eu^{3+} ions asymmetry variation in different local environment and normally becomes larger with increasing interaction of the Eu^{3+} with its neighbours due to the decrease in its site symmetry.[50,51] The largest intensity ratio (3.60) was observed for 1 : 1 Eu(**L**)$_1$. It reflects that the lower symmetry of the Eu^{3+} and hence a larger Eu^{3+}–**L** interaction of the complexes, implying a more complete coordination between Eu^{3+} to terpyridine ligand.

Table 1 Photophysical data of the samples Eu(**L**)$_n$

L : Eu^{3+}	τ [ms]	n_w	R
3 : 1	0.30	3.37	3.20
2 : 1	0.33	2.71	3.24
1 : 1	0.36	2.36	3.60
1 : 2	0.25	3.78	3.01
1 : 3	0.24	4.00	2.89

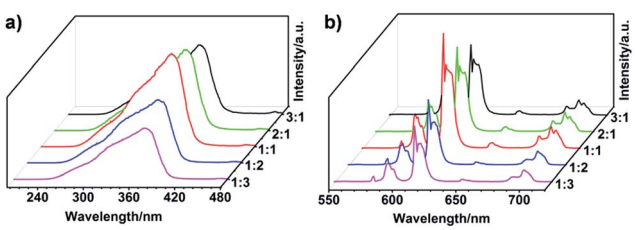

Fig. 5 (a) Excitation spectra monitored at 613 nm and (b) emission spectra excited at 360 nm of the samples in the solid state: L to Eu^{3+} ratio from 3 : 1 to 1 : 3.

2.3 Sensing of low-level water in organic solvents

The attractive dynamic properties of metal-coordination bonds make the complexes highly interesting for preparing stimuli-responsive smart materials for such bonds provide unique environmental sensibility.[52,53] Ln^{3+}–N interactions are typically weaker than Ln^{3+}–O interactions,[54] which indicates that Eu^{3+}–N coordination bonds in the complex in this study are easily affected by water molecules and hence the luminescence can tend to be quenched through vibrational coupling with high O–H vibration overtones in or near the first coordination spheres. Thus, the as-synthesized samples can be used to detect water content in organic solvents. Since we have known that the sample with **L** to Eu^{3+} molar ratio being 1 : 1 (Eu(**L**)$_1$) shows much stronger emission intensity and much longer decay times than that with other molar ratios, we therefore test the performance of Eu(**L**)$_1$ as a luminescent sensor of moisture in organic solvents. The exposure of Eu(**L**)$_1$ to the vapors of ether containing aliquots of water (0–5% v/v) for 20 min leads to obvious reduction in the brightness of the emission light and the remarkable changes in emission color as shown in Fig. 6a, which reveals that the bright emission color becomes yellowish when the water level in ether is up to 5%. The observed emission colors match well with the calculated chromaticity coordinates based on the CIE (Commission Internationaled' Eclairage) chromaticity diagram and can be easily and directly observed by naked eyes under an UV lamp (Fig. 6b). Their corresponding emission intensity of $^5D_0 \rightarrow {}^7F_2$ decreases gradually with the increase of water in ether as shown in Fig. 6c and d. The histogram in Fig. 6c clearly shows that even a very small amount (0.1%, v/v) of H_2O to anhydrous ether cause about 6% decrease of the emission intensity. When the water content is up to 5% (v/v), the emission intensity is decreased to 8% of its original value. Furthermore, the emission intensity ratio R of 613 nm ($^5D_0 \rightarrow {}^7F_2$) and 591 nm ($^5D_0 \rightarrow {}^7F_1$) changes remarkably as the water content changes. It reduces from 2.65 for the pure ether to 1.17 for that containing 5% (v/v) water (Table S1, ESI†), indicating that the symmetry of the Eu^{3+} sites has changed remarkably, possibly caused by the coordination of water molecules to Eu^{3+} ions *via* the replacement of **L**, owing to the

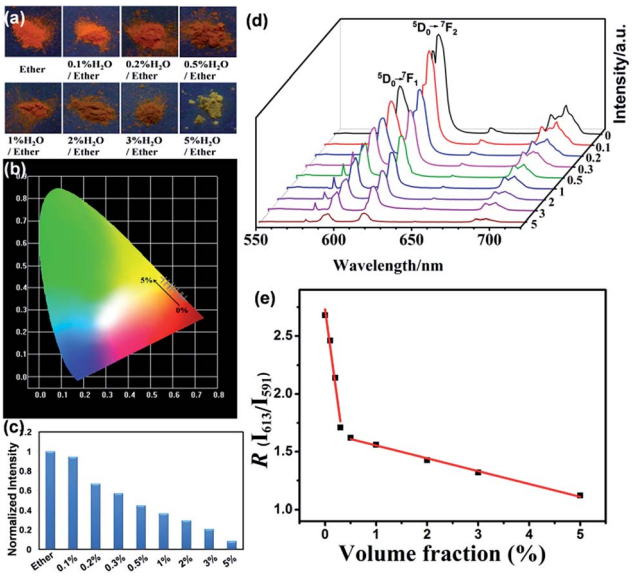

Fig. 6 Photophysical parameters of Eu(L)$_1$ after exposure to ether with increasing amount of water (0% to 5%, volume fraction): (a) digital photographs under near UV irradiation at 365 nm; (b) CIE chromaticity coordinates; (c) normalized luminescence emission intensity at 613 nm; (d) emission spectra excited at 360 nm; (e) two-separated fitted curves between R and the water molecular content in ether (0–5%, v/v).

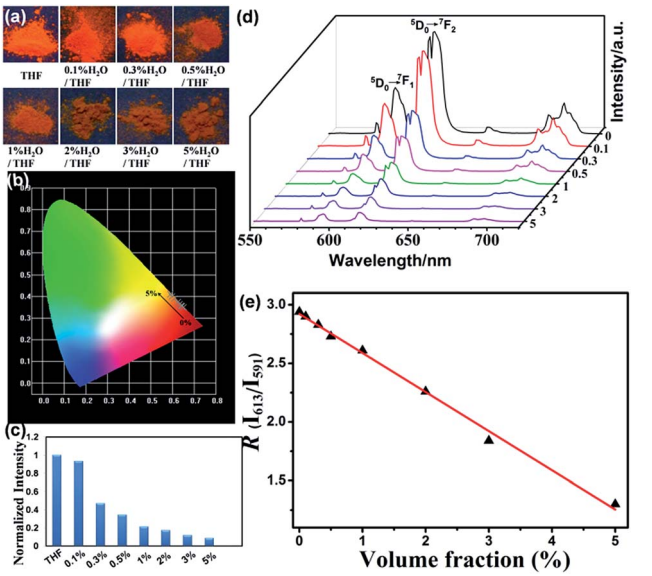

Fig. 7 Photophysical parameters of Eu(L)$_1$ after exposure to THF with increasing amount of water (0% to 5%, volume fraction): (a) digital photographs under near UV irradiation at 365 nm; (b) CIE chromaticity coordinates; (c) normalized luminescence emission intensity at 613 nm; (d) emission spectra excited at 360 nm; (e) the fitted curve between R and the water molecular content in THF (0–5%, v/v).

dynamical feature of N–Eu^{3+} coordination bonds. This can be further supported by the decrease of the luminescence decay time calculated from the decay curves as shown in Table S1.† Interestingly, two-separated linear fitting in Fig. 6e shows that R is changed linearly with the increasing water concentrations added to ether solution, the functions are shown in Table S2 (ESI†), with a correlation coefficient of 0.993. This indicates that Eu(**L**)$_1$ is an excellent self-calibrated luminescent sensor for quantitative analysis of water in ether, which can make the water molecular detection independent of the local environment, thus conquering the main disadvantages of single emission intensity-based measurements.[55,56]

Eu(**L**)$_1$ is also tested as a moisture sensor in THF. The photophysical parameters such as luminescence colors, emission intensity and chromaticity coordinates change along with the variation of water content in THF are shown in Fig. 7. The variations of R and luminescence lifetime of Eu(**L**)$_1$ are decreased as water increases from 0% to 5% v/v (Table S3, ESI†). The linear relationship between R and the water molecular content in THF (0–5%, v/v) could be fitted to the function shown in Fig. 7e and Table S2 (ESI†).

2.4 Temperature-dependent photoluminescence

The luminescent behavior of the complex can also be tuned by temperature variation and the temperature dependent luminescence spectra of Eu(**L**)$_1$ are shown in Fig. 8. When the temperature varies from 80 to 300 K ($\Delta T = 20$ K), the emission peak remains unchanged, while the normalized luminescence intensity of $^5D_0 \rightarrow {}^7F_2$ transition at 613 nm band is gradually

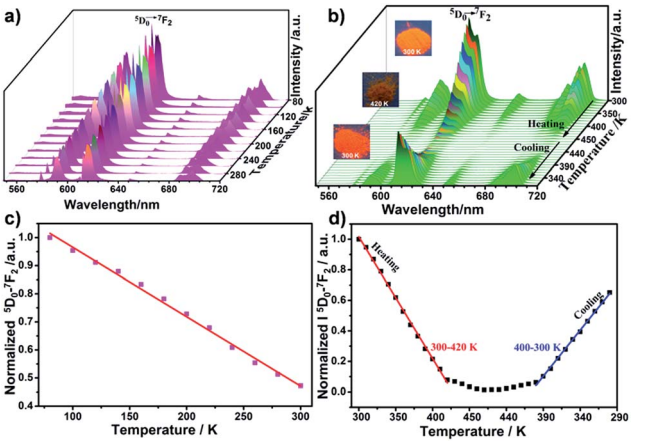

Fig. 8 Temperature-dependent emission spectra and normalized luminescence intensity of Eu(L)$_1$ within the temperature ranging from 80–300 K (a and b) and the temperature in heating process from 300–470 K and cooling process from 450–300 K (c and d). The red and blue lines are the fitting curves. Inset: digital photographs (taken under illumination with 365 nm UV light) of Eu(L)$_1$ powder.

decreased (Fig. 8a). The temperature (T_1) can be linearly related to the luminescence intensity (I_1) within the range from 80 to 300 K by eqn (1) with a correlation coefficient of 0.995 (Fig. 8b):

$$T_1 = 491.1 - 405I_1 \quad (1)$$

Remarkably, approximately 53% of the luminescence intensity of the Eu^{3+} center decreased with a stepwise increase in temperature from 80 to 300 K, and the change in intensity

ratio was 0.24% per K (Table S4, ESI†). In addition, the temperature sensibility of Eu(**L**)$_1$ can further be confirmed by the luminescence lifetime, which is decreased from 0.22 ms to 0.18 ms when the temperature enhanced from 80 to 300 K.

The aforementioned properties make the as-synthesized complex Eu(**L**)$_1$ a potential candidate for temperature-sensing from cryogenic temperatures to room temperature. Very interestingly, it shows excellent sensibility for the temperature range from room temperature up to 470 K. Fig. 8c shows that the luminescence intensity at 613 nm band decreases profoundly by more than 98% upon raising the temperature from 300 to 470 K. The luminescence intensity of Eu(**L**)$_1$ gradually decreased with a stepwise increase in temperature. In addition, the change in luminescence performance was easily visible by the naked eye on excitation under UV lamp (Fig. 8c, inset). Moreover, the relation between the normalized luminescence intensity (I_2) and temperature (T_2) in the range from 300 K to 420 K ($\Delta T = 10$ K) present a good linearity (eqn (2), $R = 0.998$, Fig. 8d):

$$T_2 = 427.4 - 125I_2 \quad (2)$$

The luminescence intensity decreases by 0.77% per K on increasing temperature (Table S4, ESI†), this indicating rather high sensitivity in wide temperature range from room temperature up to high temperatures.

Although several luminescence-based thermometers with a wide operating range have been reported,[57–61] single Eu^{3+}-containing luminescent thermometers with a linear response over the temperature range from cryogenic temperatures to high temperature are rarely reported. The sample we present in this work allows for the design of a thermometer with an excellent linear response to temperature over a wide range, from 80 to 420 K with a high relative sensitivity of 0.52% per K at 300 K and an unprecedented high sensitivity of 10.26% per K at 420 K (Fig. S3, ESI†).[62–64] It is clear that these values are 5–40 times higher than which previously reported in ref. 65 and are rarely observed for luminescence thermometry. These results indicate that Eu(**L**)$_1$ is an excellent and useful luminescent thermometer.

It worthy to note that the emission intensity of Eu(**L**)$_1$ was almost fully quenched at 420 K as shown in Fig. 8c, which was normally caused by the thermal activation of nonradiative deactivation pathways.[62,66,67] However, the dissociation of the Eu–**L** bond could not be excluded.[65,68] The attractive dynamic property of Eu–**L** coordination bond makes Eu(**L**)$_1$ reveal good temperature-dependent luminescence behavior. As shown in Fig. 9, heating and cooling can result in the dissociation and formation of the dynamic bond. To further verify the reversibility of the dynamic connection of Eu^{3+} and **L**, we also detect the luminescence behavior of the complex with a stepwise decrease in temperature from 450 to 300 K ($\Delta T = 10$ K) after the environmental temperature of Eu(**L**)$_1$ was heated to 470 K. Interesting, the emission intensity of Eu(**L**)$_1$ was gradually increased and recovered to 66.3% of its original value as shown in Fig. 8d, implying that the re-formation of Eu^{3+}–**L** complexes, which is in good agreement with our assumption. The relationships between the normalized luminescence intensity (I_3) of the complex and temperature (T_3) in cooling process were established and linearly fitted to the function shown in Table S4 (ESI†), with the correlation coefficient reach up to 0.998. The luminescence intensity decreases by 0.59% per K on stepwise decreasing temperature. The result indicates that Eu(**L**)$_1$ also has high sensitivity in wide range of temperature in the cooling process.

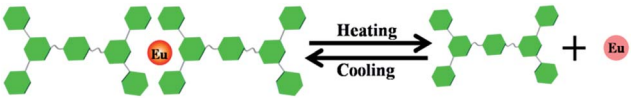

Fig. 9 The dynamic interaction of Eu(III) and **L** in the heating and cooling process.

3. Experimental

3.1 Materials

$EuCl_3 \cdot 6H_2O$ (99.99%) was purchased from Beijing HWRK Chem and **L** (96%) was purchased from Sigma-Aldrich. They were used without further purification.

3.2 Mechanochemical synthesis of Eu(**L**)$_1$

L (27.0 mg, 0.05 mmol) and $EuCl_3 \cdot 6H_2O$ (18.3 mg, 0.05 mmol) were manually ground in a mortar with a pestle for 10 min.

3.3 Exposure to organic solvents (water content from 0 to 5% v/v)

The powder samples of Eu(**L**)$_1$ were prepared for the detecting experiments. For each experiment, 200 mg Eu(**L**)$_1$ were put in a small bottle and exposed to solvents (water content from 0% to 5%, v/v). The powder samples (Eu(**L**)$_1$) and the small bottle were placed into a sealed container (about 100 mL), which contains about 4 mL organic solvent for 1 h.

3.4 Characterization

Infrared (IR) spectra were obtained with a Bruker Vector 22 spectrophotometer by using KBr pellets for solid samples from 400 to 4000 cm^{-1} at a resolution of 4 cm^{-1}. Elemental analysis was performed on an Elementar Vario EI system. SEM images were obtained from a FE-SEM (Hitachi S-4300) at an acceleration voltage of 10 kV. Samples on quartz substrate were directly put in the chamber of the instrument, for the photophysical measurements. The steady-state luminescence spectra and the lifetime measurements were measured on an Edinburgh Instruments FS920P spectrometer. Absolute quantum yield measurements were carried on the aforementioned fluorescence spectrophotometer equipped with an integrating sphere. A UV-visible Agilent Cray 100 spectrometer, with a quartz cuvette with path length 10 mm, was used to determine the wavelength of the maximum UV absorbance peak. The absorbance was measured from 200 to 800 nm.

4. Conclusions

In summary, a solid state Eu^{3+} complex was successfully synthesized by mechanochemical synthetic method. Without using any solvents and requiring only a few minutes, the single-step mechanochemical reaction serves as a "green" approach to prepare complex by the self-assembly process between Eu^{3+} and bis-terpyridine compound. Remarkably, all photophysical data reported herein point towards the same conclusion that $Eu(\mathbf{L})_1$ (ligand : Eu^{3+} = 1 : 1) shows the best luminescence performance and well stimuli-responsiveness (including temperature, moisture). $Eu(\mathbf{L})_1$ can act as a highly efficient luminescent sensor for detecting, in real time, traces of water (0.1–5% v/v) in ether and THF, which is based on the ratiometric luminescence determination method. Furthermore, $Eu(\mathbf{L})_1$ reveals excellent linear correlation between emission intensity and temperature ratio from 80–300 K, and 300–420 K, with high relative sensitivity values of 0.52% per K at 300 K and 10.26% per K at 420 K, enabling it to be a candidate for luminescent thermometer. Surprisingly, the emission intensity of the complex can be recovered to 66.3% of its original value in the cooling process from 450 to 300 K, which is attributed to the re-formation of Eu–**L**, making $Eu(\mathbf{L})_1$ as an unprecedentedly smart material. We believe that our strategy will open up a new perspective for the development of luminescent complexes in the near future.

Acknowledgements

This work was financially supported by the National Natural Science Foundation of China (21271060, 21502039, 21236001, 21605036), the Hebei Natural Science Foundation (B2016202147, B2016202149), the Graduate outstanding innovative topics of Hebei Province (220056) and the Educational Committee of Hebei Province (LJRC021).

References

1 X. Huang, S. Han, W. Huang and X. Liu, *Chem. Soc. Rev.*, 2012, **42**, 173–201.
2 S. Eliseeva and J. C. G. Buenzli, *Chem. Soc. Rev.*, 2010, **39**, 189–227.
3 Y. Yang, Q. Zhao, W. Feng and F. Li, *Chem. Rev.*, 2012, **113**, 192–270.
4 Y. Ding, Y. Wang, H. Li, Z. Duan, H. Zhang and Y. Zheng, *J. Mater. Chem.*, 2011, **21**, 14755–14759.
5 N. Sabbatini, M. Guardigli and J. M. Lehn, *Coord. Chem. Rev.*, 1993, **123**, 201–228.
6 D. Yang, Y. Wang, L. He and H. Li, *ACS Appl. Mater. Interfaces*, 2016, **8**, 19709–19715.
7 C. Tschierske, *Angew. Chem., Int. Ed.*, 2000, **39**, 2454–2458.
8 Q. Zheng, Z. Ma and S. Gong, *J. Mater. Chem. A*, 2016, **4**, 3324–3334.
9 T. Suzuki, T. Sato, J. Zhang, M. Kanao, M. Higuchi and H. Maki, *J. Mater. Chem. C*, 2016, **4**, 1594–1598.
10 R. K. Pandey, M. Delwar Hossain, C. Chakraborty, S. Moriyama and M. Higuchi, *Chem. Commun.*, 2015, **51**, 11012–11014.
11 R. K. Pandey, M. D. Hossain, S. Moriyama and M. Higuchi, *J. Mater. Chem. A*, 2014, **2**, 7754–7758.
12 A. Wild, A. Winter, F. Schlutter and U. S. Schubert, *Chem. Soc. Rev.*, 2011, **40**, 1459–1511.
13 S. Hornig, I. Manners, G. R. Newkome and U. S. Schubert, *Macromol. Rapid Commun.*, 2010, **31**, 771–771.
14 C. Rajadurai, O. Fuhr, R. Kruk, M. Ghafari, H. Hahn and M. Ruben, *Chem. Commun.*, 2007, **25**, 2636–2638.
15 A. Duerrbeck, S. Gorelik, J. Hobley, J. E. Wu, A. Hor and N. Long, *Chem. Commun.*, 2015, **51**, 8656–8659.
16 O. Kotova, R. Daly, C. M. G. dos Santos, M. Boese, P. E. Kruger, J. J. Boland and T. Gunnlaugsson, *Angew. Chem., Int. Ed.*, 2012, **51**, 7208–7212.
17 T. Sato and M. Higuchi, *Chem. Commun.*, 2012, **48**, 4947–4949.
18 G. Lyu, Q. Zhang, J. I. Urgel, G. Kuang, W. Auwarter, D. Ecija, J. V. Barth and N. Lin, *Chem. Commun.*, 2016, **52**, 1618–1621.
19 M. Martínez-Calvo, O. Kotova, M. E. Möbius, A. P. Bell, T. McCabe, J. J. Boland and T. Gunnlaugsson, *J. Am. Chem. Soc.*, 2015, **137**, 1983–1992.
20 J. R. Kumpfer, J. Jin and S. J. Rowan, *J. Mater. Chem.*, 2010, **20**, 145–151.
21 W. Weng, J. B. Beck, A. M. Jamieson and S. J. Rowan, *J. Am. Chem. Soc.*, 2006, **128**, 11663–11672.
22 A. J. McConnell, C. S. Wood, P. P. Neelakandan and J. R. Nitschke, *Chem. Rev.*, 2015, **115**, 7729–7793.
23 P. Chen, Q. Li, S. Grindy and N. Holten-Andersen, *J. Am. Chem. Soc.*, 2015, **137**, 11590–11593.
24 Z. Zhang, Y.-N. He, L. Liu, X.-Q. Lu, X.-J. Zhu, W.-K. Wong, M. Pan and C.-Y. Su, *Chem. Commun.*, 2016, **52**, 3713–3716.
25 V. A. Friese and D. G. Kurth, *Coord. Chem. Rev.*, 2008, **252**, 199–211.
26 P. Wei, X. Yan and F. Huang, *Chem. Soc. Rev.*, 2015, **44**, 815–832.
27 G. Yu, K. Jie and F. Huang, *Chem. Rev.*, 2015, **115**, 7240–7303.
28 X. Ma, G. K. Lim, K. D. M. Harris, D. C. Apperley, P. N. Horton, M. B. Hursthouse and S. L. James, *Cryst. Growth Des.*, 2012, **12**, 5869–5872.
29 D. E. Crawford and J. Casaban, *Adv. Mater.*, 2016, **28**, 5747–5754.
30 A. Kobayashi, T. Hasegawa, M. Yoshida and M. Kato, *Inorg. Chem.*, 2016, **55**, 1978–1985.
31 A. D. Katsenis, A. Puškarić, V. Štrukil, C. Mottillo, P. A. Julien, K. Užarević, M.-H. Pham, T.-O. Do, S. A. J. Kimber, P. Lazić, O. Magdysyuk, R. E. Dinnebier, I. Halasz and T. Friščić, *Nat. Commun.*, 2015, **6**, 1–6.
32 S. L. James, C. J. Adams, C. Bolm, D. Braga, P. Collier, T. Friscic, F. Grepioni, K. D. M. Harris, G. Hyett, W. Jones, A. Krebs, J. Mack, L. Maini, A. G. Orpen, I. P. Parkin, W. C. Shearouse, J. W. Steed and D. C. Waddell, *Chem. Soc. Rev.*, 2012, **41**, 413–447.
33 P. J. Beldon, L. Fábián, R. S. Stein, A. Thirumurugan, A. K. Cheetham and T. Friščić, *Angew. Chem., Int. Ed.*, 2010, **49**, 9640–9643.
34 K. Užarević, T. C. Wang, S.-Y. Moon, A. M. Fidelli, J. T. Hupp, O. K. Farha and T. Friščić, *Chem. Commun.*, 2016, **52**, 2133–2136.

35 T. Friščić, D. G. Reid, I. Halasz, R. S. Stein, R. E. Dinnebier and M. J. Duer, *Angew. Chem.*, 2010, **122**, 724–727.
36 T. Friščić, *Chem. Soc. Rev.*, 2012, **41**, 3493–3510.
37 A. L. Garay, A. Pichon and S. L. James, *Chem. Soc. Rev.*, 2007, **36**, 846–855.
38 S. L. James, C. J. Adams, C. Bolm, D. Braga, P. Collier, T. Friščić, F. Grepioni, K. D. Harris, G. Hyett and W. Jones, *Chem. Soc. Rev.*, 2012, **41**, 413–447.
39 M. Ferguson, N. Giri, X. Huang, D. Apperley and S. L. James, *Green Chem.*, 2014, **16**, 1374–1382.
40 E. C. Constable, *Chem. Soc. Rev.*, 2007, **36**, 246–253.
41 D. Wang, H. Wang and H. Li, *ACS Appl. Mater. Interfaces*, 2013, **5**, 6268–6275.
42 P. Zhang, Y. Wang, H. Liu and Y. Chen, *J. Mater. Chem.*, 2011, **21**, 18462–18466.
43 R. López, D. Villagra, G. Ferraudi, S. Moya and J. Guerrero, *Inorg. Chim. Acta*, 2004, **357**, 3525–3531.
44 A. Duerrbeck, S. Gorelik, J. Hobley, A. M. Yong, G. S. Subramanian, A. Hor and N. Long, *J. Mater. Chem. C*, 2015, **3**, 8992–9002.
45 P. Cao, O. Khorev, A. Devaux, L. Sägesser, A. Kunzmann, A. Ecker, R. Häner, D. Brühwiler, G. Calzaferri and P. Belser, *Chem.–Eur. J.*, 2016, **22**, 4046–4060.
46 A. Devaux, G. Calzaferri, P. Belser, P. Cao, D. Brühwiler and A. Kunzmann, *Chem. Mater.*, 2014, **26**, 6878–6885.
47 M. P. Oude Wolbers, F. C. van Veggel, B. H. Snellink-Ruël, J. W. Hofstraat, F. A. Geurts and D. N. Reinhoudt, *J. Am. Chem. Soc.*, 1997, **119**, 138–144.
48 C. Bischof, J. Wahsner, J. Scholten, S. Trosien and M. Seitz, *J. Am. Chem. Soc.*, 2010, **132**, 14334–14335.
49 D. D'Alessio, S. Muzzioli, B. W. Skelton, S. Stagni, M. Massi and M. I. Ogden, *Dalton Trans.*, 2012, **41**, 4736–4739.
50 D. Yang, Y. Wang, Y. Wang, Z. Li and H. Li, *ACS Appl. Mater. Interfaces*, 2015, **7**, 2097–2103.
51 D. Yang, Y. Wang, Y. Wang and H. Li, *Sens. Actuators, B*, 2016, **235**, 206–212.
52 P. Chen and N. Holten-Andersen, *Adv. Opt. Mater.*, 2015, **3**, 1041–1046.
53 M. Chiper, R. Hoogenboom and U. S. Schubert, *Macromol. Rapid Commun.*, 2009, **30**, 565–578.
54 J. H. Forsberg, *Coord. Chem. Rev.*, 1973, **10**, 195–226.
55 P. Li, Z. Li and H. Li, *Adv. Opt. Mater.*, 2016, **4**, 156–161.
56 M. Yao and W. Chen, *Anal. Chem.*, 2011, **83**, 1879–1882.
57 T. Wang, P. Li and H. Li, *ACS Appl. Mater. Interfaces*, 2014, **6**, 12915–12921.
58 Z. Li, Z. Hou, D. Ha and H. Li, *Chem.–Asian J.*, 2015, **10**, 2720–2724.
59 C. D. Brites, P. P. Lima, N. J. Silva, A. Millán, V. S. Amaral, F. Palacio and L. D. Carlos, *Nanoscale*, 2013, **5**, 7572–7580.
60 X. Xu, Z. Wang, P. Lei, Y. Yu, S. Yao, S. Song, X. Liu, Y. Su, L. Dong and J. Feng, *ACS Appl. Mater. Interfaces*, 2015, **7**, 20813–20819.
61 K. Miyata, Y. Konno, T. Nakanishi, A. Kobayashi, M. Kato, K. Fushimi and Y. Hasegawa, *Angew. Chem., Int. Ed.*, 2013, **52**, 6413–6416.
62 S. N. Zhao, L. J. Li, X. Z. Song, M. Zhu, Z. M. Hao, X. Meng, L. L. Wu, J. Feng, S. Y. Song and C. Wang, *Adv. Funct. Mater.*, 2015, **25**, 1463–1469.
63 A. Cadiau, C. D. Brites, P. M. Costa, R. A. Ferreira, J. Rocha and L. D. Carlos, *ACS Nano*, 2013, **7**, 7213–7218.
64 C. D. Brites, P. P. Lima, N. J. Silva, A. Millán, V. S. Amaral, F. Palacio and L. D. Carlos, *Nanoscale*, 2012, **4**, 4799–4829.
65 X.-d. Wang, O. S. Wolfbeis and R. J. Meier, *Chem. Soc. Rev.*, 2013, **42**, 7834–7869.
66 Y. Cui, F. Zhu, B. Chen and G. Qian, *Chem. Commun.*, 2015, **51**, 7420–7431.
67 X. Rao, T. Song, J. Gao, Y. Cui, Y. Yang, C. Wu, B. Chen and G. Qian, *J. Am. Chem. Soc.*, 2013, **135**, 15559–15564.
68 J. B. Beck and S. J. Rowan, *J. Am. Chem. Soc.*, 2003, **125**, 13922–13923.

